Clays and Clay Minerals, Vol. 67, No. 4:340–347, 2019

PHOTOCATALYTIC DEGRADATION OF METHYLENE BLUE OVER LAYERED DOUBLE HYDROXIDES USING VARIOUS DIVALENT METAL IONS

Guoxiang Pan[1,2]*, Minhong Xu[1], Kai Zhou[1], Yue Meng[1], Haifeng Chen[1], Yuhua Guo[1], and Tao Wu[1]

[1]Department of Materials Engineering, Huzhou University, Huzhou 313000, People's Republic of China
[2]Zhejiang Huayuan Pigment Co., Ltd, Deqing 313220, People's Republic of China

Abstract—To apply hydrotalcites more effectively to the problem of dye wastewater, the effects of divalent metal ions on the structure and stability of hydrotalcites, especially on their photocatalytic activity, were compared. In the present study, *M*/Cr hydrotalcites (M_3Cr-CO_3-LDHs) (in which *M* = Mg, Co, Ni, Cu, Zn), where the *M*/Cr molar ratio was 3, were prepared by the co-precipitation method. The structures and properties were characterized using powder X-ray diffraction (XRD), Fourier-transform infrared spectroscopy (FTIR), thermogravimetric-differential thermal analysis (TG-DTA), and UV-Visible diffuse reflectance spectroscopy (UV-Vis DRS). The results showed that five kinds of M_3Cr-CO_3-LDHs were synthesized successfully, and the layered structure of the samples obtained was regular and the crystal phase was single. When methylene blue (MB) solution was exposed to ZnCr-CO_3-LDHs, H_2O_2, and visible light irradiation, more than 90.67% of the methylene blue (MB) was removed after 140 min. The photocatalytic activity of the samples was in the order: Co_3Cr-CO_3-LDHs > Mg_3Cr-CO_3-LDHs > Cu_3Cr-CO_3-LDHs > Zn_3Cr-CO_3-LDHs > Ni_3Cr-CO_3-LDHs. The results of a catalytic mechanism study showed that photocatalytic degradation of MB involved a demethylation reaction, with the reactive species containing $\bullet O_2^-$, •OH, and h^+.

Keywords—Co-precipitation Method · M_3Cr-CO_3-LDHs · Methylene Blue · Photocatalytic Degradation

INTRODUCTION

Dye wastewater is industrial waste which is difficult to deal with because of its high concentration, poor biodegradability, and high chromaticity (Xia et al. 2014; Kuzyaka et al. 2018). With the rapid development of printing and dyeing industries, the increase in wastewater emissions has led to a sharp decline in water quality in the natural environment (Shang et al. 2017). In addition, if dye wastewater is discharged to the environment without timely treatment, a series of chemical reactions is generated which produces toxic by-products, which worsen the ecological situation (Crossland et al. 2013; Alijani et al. 2017; Bohac & Bujdak 2018; Karataş et al. 2018). Photocatalytic degradation is a relatively recent technology which is showing significant potential in terms of its ability to control pollution (Ray et al. 2017; Adeleke et al. 2018). Identifying efficient catalysts for organic dye wastewater treatment is vitally important.

Hydrotalcites are anionic layered clay materials (layered double hydroxides, LDHs) and the molecular formula of a typical hydrotalcite-like compound is $Mg_6Al_2(OH)_{16}CO_3{\cdot}4H_2O$. Mg^{2+} and Al^{3+} in LDHs can be replaced in the structure isomorphously by other divalent and trivalent cations (Zhou et al. 2016). The general formula of the compound is $[M^{2+}_{1-x}M^{3+}_x(OH)_2]^{x+}(A^{n-})_{x/n}{\cdot}mH_2O$, in which A^{n-} represents interlayer anions, x is the ratio $M^{3+}/(M^{2+}+M^{3+})$, and m is the quantity of crystal water (Pan et al. 2012; Vialat et al. 2013). Because LDHs have an exchangeable anion structure, adjustable pore size, thermal stability, and other properties, it can be used in catalysis, medicine, and other industries (Zhou & Keeling 2013; Gao et al. 2018; Li et al. 2018) New types of hydrotalcite have been synthesized by changing the metal cations and anions in the hydrotalcite structure, such as Mg/Al/Ce LDHs, Cu-Mg-Al LDHs, and Mg-Al LDHs doped with Tb etc. (Wang et al. 2011; Chen et al. 2016; Comelli et al. 2018; Xu et al. 2019). Research into the application of photocatalytic activity of LDHs has become important (Zhou 2010; Zhang et al. 2018). Photocatalytic degradation of pesticides was studied by Da et al. (2014) using decatungstate intercalated macroporous layered double hydroxides. Visible light-promoted degradation of gaseous volatile organic compounds catalyzed by Au supported on layered double hydroxides was studied by Fu et al. (2019).

In order to evaluate the exchangeability of cations on hydrotalcite laminates (Mao et al. 2017) and to maximize the potential of hydrotalcites in the dye wastewater treatment, the effects of divalent metal ions on the structure, stability, and photocatalytic activity of hydrotalcites were assessed. To this end, *M*/Cr hydrotalcite (M_3Cr-CO_3-LDHs, where *M* = Mg, Co, Ni, Cu, or Zn), with an *M*/Cr atomic ratio of 3, was prepared by the co-precipitation method. Photocatalytic performance is assessed by measuring the degradation of MB aqueous solutions under visible irradiation. The effects of irradiation time, catalyst type, and reuse performance of MB degradation were investigated and the reaction mechanism was studied also.

EXPERIMENTAL

Materials

For the present study, analytically pure $M(NO_3)_2{\cdot}6H_2O$ (*M* is Co, Mg, Ni, Zn, Cu), $Cr(NO_3)_3{\cdot}9H_2O$, Na_2CO_3, NaOH,

* E-mail address of corresponding author: pgxzjut@163.com
DOI: 10.1007/s42860-019-00031-2

This paper was originally presented during the World Forum on Industrial Minerals, held in Qing Yang, China, October 2018.

isopropanol, p-benzoquinone, ethylene diamine tetraacetic acid disodium salt, H_2O_2, and MB were purchased from Aladdin Reagent Co., Ltd (Shanghai, China). All solutions were prepared with deionized water.

Preparation of M_3Cr-CO_3-LDHs

A series of M_3Cr-CO_3-LDHs was synthesized employing the co-precipitation method (Pan et al. 2012). Using a M/Cr molar ratio of 3.0, known amounts of $M(NO_3)_2{\cdot}6H_2O$ and $Cr(NO_3)_3{\cdot}9H_2O$ solid were dissolved in boiling water to be used as solution A. Then, 6.40 g of NaOH and 1.06 g of Na_2CO_3 were dissolved in boiling water as solution B. Under constant stirring, solutions A and B were added drop-wise to a beaker which was filled with deionized water. In this process, the mixed solution was adjusted using NaOH solution until the pH was between 9 and 10. The solution was then stirred continuously for 30 min. Finally, the slurry obtained was aged at 65°C for 24 h. The resulting precipitates were centrifuge washed with deionized water. After that, the samples were dried overnight at 65°C, and they were labeled using the format M_3Cr-CO_3-LDH.

Structural Characterization

X-ray diffraction patterns of the samples were recorded an XD-6 instrument using CuKα radiation (Beijing Purkinje General Instrument Co., Ltd., Beijing, China). Infrared spectra were recorded using the KBr disc method on a Nicolet 5700 FTIR spectrophotometer (Thermo Scientific, Waltham, Massachusetts, USA). The thermal properties of the samples were measured using a CRY-2P instrument (Beijing Henven scientific instrument factory, Beijing, China); the heating rate was 10°C/min and the temperature range was 25–800°C. UV-Vis diffuse reflectance spectra (UV-Vis DRS) of the samples were tested using a UV4100 UV-Vis spectrophotometer (Thermo Scientific, Waltham, Massachusetts, USA); $BaSO_4$ was used as a reference standard. The time-dependent UV-Vis spectra of MB solutions were measured using a Shimadzu UV-2600 UV-Vis spectrophotometer (Tokyo, Japan).

Catalytic Experiments

The photocatalytic properties of ZnCr-CO_3-LDHs were determined by photodegradation of MB solution under visible light irradiation using a 150 W halogen lamp. A photocatalyst (0.5 g) was mixed with 25 mL of 5 mg/L MB aqueous solution with an additional 0.5 mL of H_2O_2. The mixed solution was stirred with a magnetic stirrer. A sample solution was taken at a given time and separated through centrifugation. The concentration of MB solution was evaluated by UV-Vis spectrophotometry at 662 nm. The degradation efficiency was calculated using the following equation:

$$D = (C_0 - C_t)/C_0 \times 100 = (A - A_t)/A \times 100\%$$

where C_0 is the initial concentration of MB solution after avoiding light, and C_t is the concentration of MB solution after a known photoreaction time, A is the initial absorbance of MB solution after avoiding light, and A_t is the absorbance of MB solution after a known photoreaction time.

RESULTS AND DISCUSSION

XRD Characterization

The regularity of the crystal structure, crystallinity, and crystal-cell parameters of the samples was tested using XRD (Chen et al. 2016). The XRD patterns of five kinds of M_3Cr-CO_3-LDHs (Fig. 1) showed that the diffraction peaks were at 11.7, 23.6, and 34.7°2θ, which corresponded to the characteristic diffraction peaks of hydrotalcite; and the crystal face indexes were (003), (006), and (009), respectively. The above-mentioned results were consistent with published information (Prevot et al. 2005; Pan et al. 2011; Yang et al. 2018; Xu et al. 2019), indicating that the five kinds of M_3Cr-CO_3-LDHs had typical layered structures. The diffraction peaks of these five kinds of M_3Cr-CO_3-LDHs were strong and sharp, which indicated that the synthesized M_3Cr-CO_3-LDHs had fine crystallinity. In addition, the diffraction peak of Zn_3Cr-CO_3-LDHs was the strongest, which showed that Zn_3Cr-CO_3-LDHs formed the best crystals. The peak observed at d_{009} in Cu_3Cr-CO_3-LDHs, however, was unidentified and indicated less crystallinity. It may have been a consequence of incomplete washing.

The layer spacing of the diffraction peak corresponding to the d_{003} plane was calculated from the Bragg equation ($n\lambda = 2d\sin\theta$), giving values for CuCr-CO_3-LDHs, ZnCr-CO_3-LDHs, NiCr-CO_3-LDHs, MgCr-CO_3-LDHs, and CoCr-CO_3-LDHs of 0.747, 0.764, 0.773, 0.765, and 0.749 nm, respectively. These data are similar to the results reported in the literature of d_{003} spacing of carbonate hydrotalcite (Sels et al. 2001; Rives et al. 2003; Tichit et al. 2006; Yang et al. 2019). Comparison of the five d_{003} results revealed that the MgCr-CO_3-LDHs layer spacing was the largest, which might be due to the fact that Mg has the smallest atomic radius.

FTIR Spectroscopy Analysis

The FTIR patterns of the five kinds of M_3Cr-CO_3-LDHs (Fig. 2) revealed five absorption peaks between 3470 and

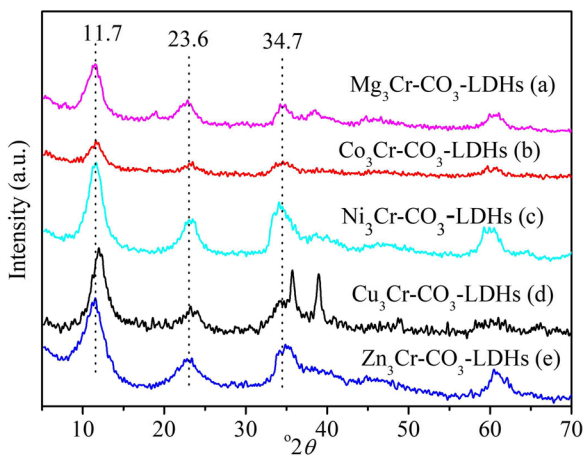

Fig. 1 XRD patterns of Mg_3Cr-CO_3-LDHs (a), Co_3Cr-CO_3-LDHs (b), Ni_3Cr-CO_3-LDHs (c), Cu_3Cr-CO_3-LDHs (d), and Zn_3Cr-CO_3-LDHs (e)

https://doi.org/10.1007/s42860-019-00031-2 Published online by Cambridge University Press

3540 cm^{-1} which were ascribed to the stretching vibration of the H_2O molecule; this was because the surface and the interlayer space of the LDHs adsorbed a certain number of H_2O molecules. Compared with the stretching vibration of free hydroxyl (at ~3650 cm^{-1}), the peak shifted to a lower wavenumber, which indicated that a hydrogen bond between layers of H_2O and the CO_3^{2-} ion and the hydroxyl group appeared. In addition, absorption peaks between 1650 and 1665 cm^{-1} were caused by the bending vibration of –OH in the crystal water. The peak at 1384–1386 cm^{-1} was ascribed to the anti-symmetric stretching vibration peak of CO_3^{2-}. Absorption peaks between 520 and 630 cm^{-1} belonged to the characteristic peak of plane-bending vibration of C-O. All the patterns showed the characteristic peaks of hydrotalcite. IR spectra further confirmed the synthesis of M_3Cr-CO_3-LDHs had typical structural characteristics of hydrotalcite.

TG-DTA Characterization

The TG-DTA curves of Mg_3Cr-CO_3-LDHs, Zn_3Cr-CO_3-LDHs, Co_3Cr-CO_3-LDHs, Ni_3Cr-CO_3-LDHs, and Cu_3Cr-CO_3-LDHs (Fig. 3a) showed that during the heating process, the thermal behavior of these compounds could be divided into two stages. In the first stage, the weight loss was ~17–25%, and in the second stage, weight loss was ~17–23%. Compared with the five kinds of compounds, Mg_3Cr-CO_3-LDHs had the largest weight loss: 23%. The comparison of DTA curves showed that the thermal decomposition of the five kinds of M_3Cr-CO_3-LDHs was due mainly to two obvious endothermic processes. An endothermic peak appeared at low temperature (i.e. 50–200°C), which corresponded to the removal of surface-adsorbed water and interlayer water. A peak also appeared at higher temperature (i.e. 265–450°C), indicating that the interlayer hydroxyl was dehydrated and interlayer CO_3^{2-} anions were decomposed or removed. These results were similar to the thermal decomposition of typical Mg-Al hydrotalcites (Hibino et al. 1995).

Comparison of second-stage DTA curves (Fig. 3b) indicated the thermal decomposition temperature of Cu_3Cr-CO_3-LDHs was the highest, which showed that the thermal stability was the best. The relative thermal stabilities of the other four kinds of hydrotalcites were in the order: Mg_3Cr-CO_3-LDHs > Ni_3Cr-CO_3-LDHs > Zn_3Cr-CO_3-LDHs ≈ Co_3Cr-CO_3-LDHs, consistent with the result reported previously (Pan et al. 2012), i.e. the order of thermal stability of hydrotalcites obtained from the second law of crystal chemistry.

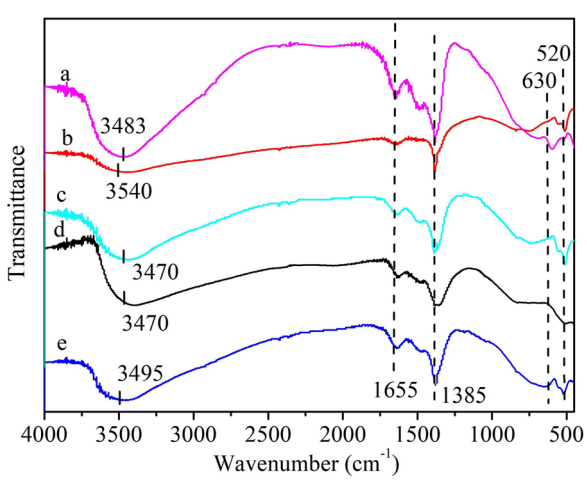

Fig. 2 FTIR patterns of Mg_3Cr-CO_3-LDHs (a), Co_3Cr-CO_3-LDHs (b), Ni_3Cr-CO_3-LDHs (c), Cu_3Cr-CO_3-LDHs (d), and Zn_3Cr-CO_3-LDHs (e)

UV-Vis DRS Analysis

The UV-Vis DRS spectra of LDHs (Fig. 4) showed that Mg_3Cr-CO_3-LDHs and Ni_3Cr-CO_3-LDHs (curve a and curve c) contained obvious absorption peaks at ~333 and 480 nm. Co_3Cr-CO_3-LDHs (curve b) had a weak absorption peak in the visible region ($\lambda > 400$ nm), but Cu_3Cr-CO_3-LDHs (curve d) had almost no absorption peaks, while Zn_3Cr-CO_3-LDHs (curve e) had obvious absorption peaks at ~410 and 560 nm. In order to utilize these kinds of catalysts effectively in visible light ($\lambda > 400$ nm), UV-Vis DRS patterns of the five kinds M_3Cr-CO_3-LDHs were compared and analyzed. The absorption region of Zn_3Cr-CO_3-LDHs was widest, next was Ni_3Cr-CO_3-LDHs, and Mg_3Cr-CO_3-LDHs and Co_3Cr-CO_3-LDHs had narrower spectra, while the absorption region of Cu_3Cr-CO_3-LDHs was narrowest. With the various divalent metal cations, the final products were different colors (Zhao et al. 2011), meaning that their absorption of visible light spanned different wavelengths and provided an incentive to explore their visible-light catalytic properties.

Photocatalytic Properties of ZnCr-CO_3-LDHs

In order to investigate the catalytic activity of ZnCr-CO_3-LDHs, MB solution was selected as the substrate for catalytic oxidation. The removal rate of MB was only 5% in the presence of ZnCr-CO_3-LDHs without visible light (Fig. 5), which was attributed to the adsorption capability of ZnCr-CO_3-LDHs (for MB). In the presence of ZnCr-CO_3-LDHs exposed to visible light, the removal rate was 10.06% after 140 min, indicating that ZnCr-CO_3-LDHs is a photocatalyst for MB degradation. When both ZnCr-CO_3-LDHs and H_2O_2 were involved in an unilluminated reaction, the removal rate of MB was 46.36% after 140 min. However, MB decreased by 49.08% when using only H_2O_2 for 140 min under visible light irradiation, which might be due to oxidation of H_2O_2. When MB solution was exposed to ZnCr-CO_3-LDHs, H_2O_2, and visible light irradiation together, >90.67% of MB was removed after 140 min. The above phenomena indicated that MB was most effectively degraded by ZnCr-CO_3-LDHs/H_2O_2 under visible light irradiation.

Reuse Performance

Repeated experiments on photodegradation of MB using ZnCr-CO_3-LDHs/H_2O_2 were performed. After each run, the photocatalysts were collected by centrifugation; distilled water was added to the centrifuge tube and stirred until the catalyst was washed washed thoroughly, and then centrifugation was continued. The process was repeated three times. After the ZnCr-CO_3-LDHs were reused three times, the degradation rates of MB solution were still >90% (Fig. 6),

https://doi.org/10.1007/s42860-019-00031-2 Published online by Cambridge University Press

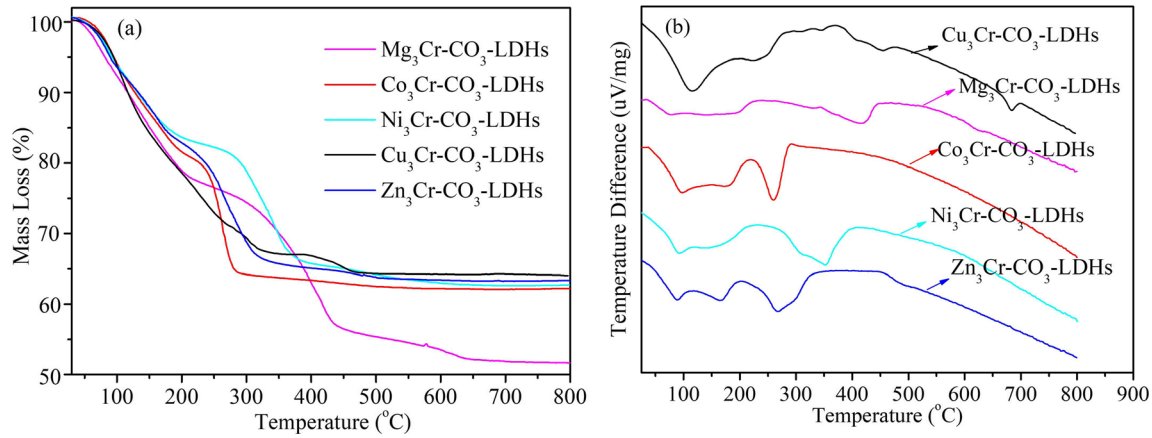

Fig. 3 TG curves of of M_3Cr-CO_3-LDHs (a), and DTA curves of M_3Cr-CO_3-LDHs (b)

indicating that ZnCr-CO_3-LDHs were stable and not photocorroded during photocatalytic reactions. In addition, when the photocatalysts were used for the second or third times, the MB was degraded rapidly. The photocatalytic degradation rate of MB was 42.65% (second attempt) and 42.14% (third attempt) after 20 min, which was faster than that of the first time of photocatalytic degradation of MB (17.76%).

The quicker degradation might be due to the transition of electrons in the valence band when using ZnCr-CO_3-LDHs in the presence of light, resulting in the formation of photogenerated electron-hole pairs on the inside and on the surface of ZnCr-CO_3-LDHs. Electrons and holes reacted with H_2O_2 to produce active species that effectively prevented recombination of electron-hole pairs, and effectively transferred electrons and holes, resulting in a series of redox reactions. In the process of reuse, visible light irradiation may activate ZnCr-CO_3-LDHs to produce photogenerated electron-hole pairs. Therefore, the reaction of photogenerated electrons and holes with H_2O_2 was accelerated and, ultimately, the degradation of MB was also accelerated.

The XRD patterns of ZnCr-CO_3-LDHs after different cycles (Fig. 7) showed that the diffraction peaks of ZnCr-CO_3-LDHs were unchanged and the peaks were similar in shape when ZnCr-CO_3-LDHs were used two or three times. The results indicated that the crystal structure of hydrotalcites did not change obviously after cyclic use, and also proved that ZnCr-CO_3-LDHs had good stability.

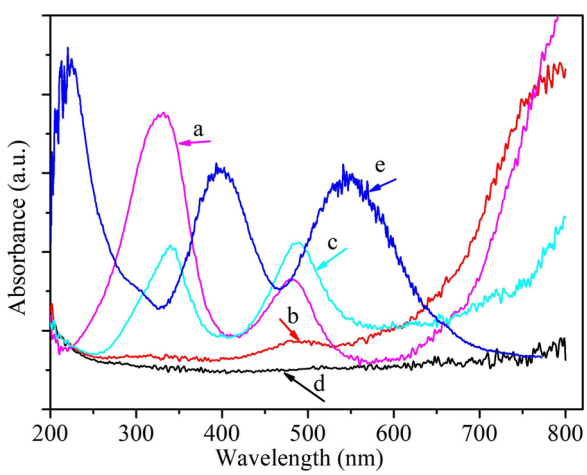

Fig. 4 UV-Vis DRS patterns of Mg_3Cr-CO_3-LDHs (a), Co_3Cr-CO_3-LDHs (b), Ni_3Cr-CO_3-LDHs (c), Cu_3Cr-CO_3-LDHs (d), and Zn_3Cr-CO_3-LDHs (e)

Catalyst Types

The photocatalytic degradation of MB with different metal ions substituted in *M*Cr-CO_3-LDHs (*M* = Zn, Mg, Co, Ni, or Cu) (Fig. 8) showed that, under the same experimental conditions, the degradation of MB with CoCr-CO_3-LDHs after 60 min was nearly 100%, while the degradation with MgCr-CO_3-LDHs and CuCr-CO_3-LDHs was >90%. But the degradation efficiencies of ZnCr-CO_3-LDHs and NiCr-CO_3-LDHs were worse; the degradation of MB was 55.78% and 48.14%, respectively, under the same conditions. When *M* was Mg, Co, or Cu, MB degraded rapidly, and a large number of bubbles was produced during the reaction. When *M* was Zn or Ni, fewer bubbles were formed. The photocatalytic activity of five kinds of M_3Cr-CO_3-LDHs was in the order: Co_3Cr-CO_3-LDHs > Mg_3Cr-CO_3-LDHs > Cu_3Cr-CO_3-LDHs > Zn_3Cr-CO_3-LDHs > Ni_3Cr-CO_3-LDHs.

Photocatalytic Mechanism

The intermediate products of MB degradation were tested (Fig. 9); the maximum absorption peak (λ = 664 nm) of MB solution decreased gradually with the prolongation of reaction time, and the maximum absorption peak shifted to λ = 651 nm. The blue shift (to lower wavelengths) of the maximum absorption wavelength of MB occurred, possibly due to the demethylation reaction found when photocatalytic degradation of MB takes place, and it removed a methyl to form azure B. According to the literature (Zhang et al. 2001), absorption bands at 654–648, 620, and 610 nm are due to MB molecular

https://doi.org/10.1007/s42860-019-00031-2 Published online by Cambridge University Press

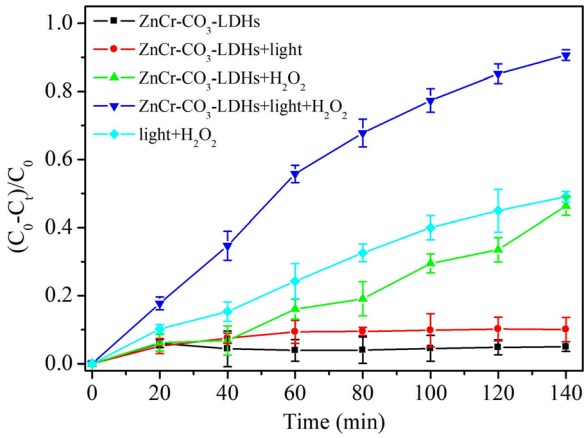

Fig. 5 Photocatalytic degradation of MB under various conditions

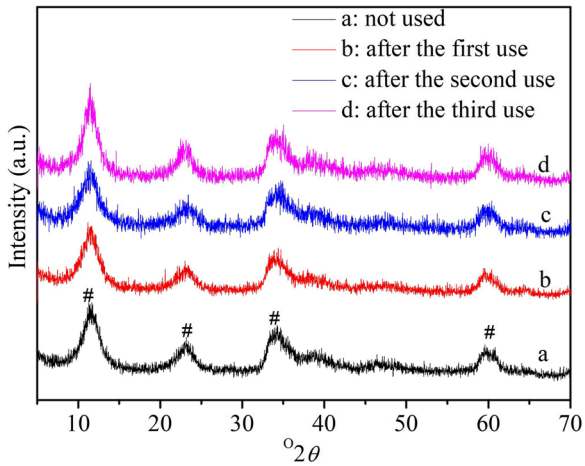

Fig. 7 XRD patterns of ZnCr-CO_3-LDHs after various cycle times

transformations to azure A, azure B, and azure C, respectively. The results of photocatalytic degradation of MB agreed with those reported in the literature. In addition, along with the prolonged irradiation time, a new absorption peak appeared in the UV region (λ = 372 nm); the absorption peak was enhanced as illumination time increased, suggesting that new substances appeared during degradation of MB.

In order to evaluate the role of these active oxidants, scavengers were added to the photocatalytic system. These were isopropanol (IPA) for •OH, p-benzoquinone (BQ) for $\bullet O_2^-$ (Yuan et al. 2015), and ethylene diamine tetraacetic acid disodium salt (EDTA-2Na) for h^+ (Xiong et al. 2012; Pan et al. 2013; Chen et al. 2014). The molar ratio of initial concentration of these three kinds of scavengers in the reaction system to MB was 200:1. The photodegradation of MB was slightly inhibited by the addition of IPA (Fig. 10). The results indicated that MB degradation was driven mainly by the participation of •OH radicals. But the reaction was accelerated when EDTA-2Na and BQ were added. The degradation rates of MB exceeded 90% after irradiation for 60 min.

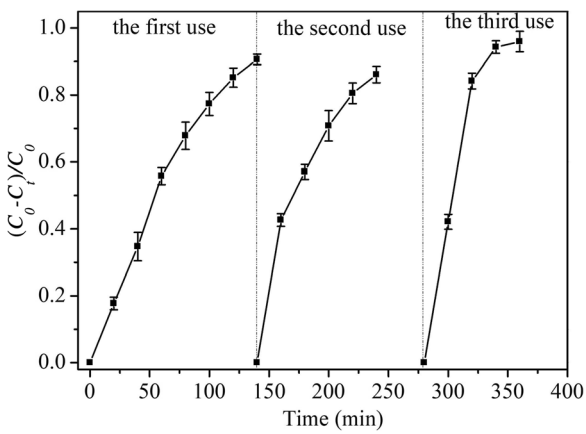

Fig. 6 Catalyst recycling study of ZnCr-CO_3-LDHs for photocatalytic degradation of MB

Based on the band theory of solids and the mechanism of semiconductor photocatalysis, researchers speculated on the possible mechanism of photocatalytic degradation of MB. Photoinduced e^-/h^+ pairs were generated on the surface of the photocatalyst ZnCr-CO_3-LDHs during irradiation (Eq. 1). H_2O_2 molecules oxidized by photoinduced h^+ were adsorbed into •OH species on the photocatalyst surface (Eq. 2), while the photoinduced e^--activated H_2O_2 and O_2 molecules were adsorbed into •OH, OH^- species on the catalyst surface (Eq. 3), and $\bullet O_2^-$ species (Eq. 4), respectively. In addition, •OH species were also generated during irradiation of H_2O_2 (Eq. 5). H_2O_2 oxidized the active $\bullet O_2^-$ species into •OH, OH^-, and O_2 species (Eq. 6). •OH and O_2 species are known to be the main active species in the photocatalytic reaction (Ishibashi et al. 2000; Xiang et al. 2011). The MB molecules were oxidized by •OH and O_2 species into small molecules (Eq. 7 and Eq. 8).

$$\text{ZnCr}-\text{CO}_3-\text{LDHs} + h\nu \rightarrow e^- + h^+ \quad (1)$$

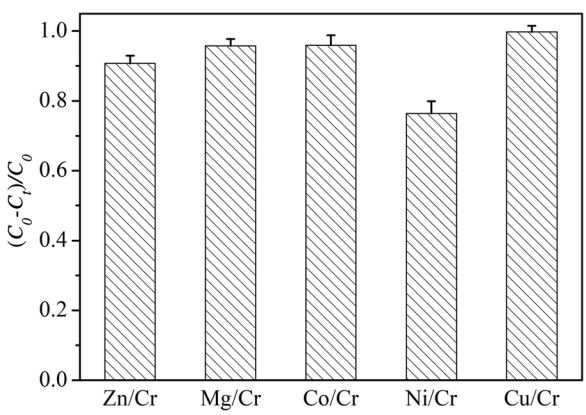

Fig. 8 Effect of catalyst types on degradation of MB

https://doi.org/10.1007/s42860-019-00031-2 Published online by Cambridge University Press

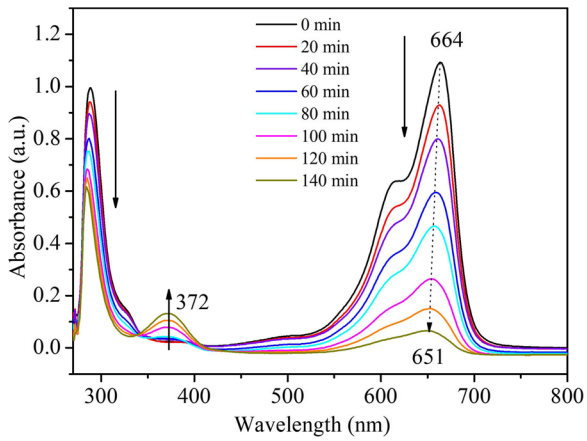

Fig. 9 UV-Vis absorption spectra of MB with different reaction times in the presence of ZnCr-CO_3-LDHs/H_2O_2 under visible light irradiation.

$$h^+ + H_2O_2 \rightarrow 2\bullet OH \quad (2)$$

$$e^- + H_2O_2 \rightarrow \bullet OH + OH^- \quad (3)$$

$$e^- + O_2 \rightarrow \bullet O_2^- \quad (4)$$

$$H_2O_2 + h\nu \rightarrow 2\bullet OH \quad (5)$$

$$\bullet O_2^- + H_2O_2 \rightarrow \bullet OH + OH^- + O_2 \quad (6)$$

$$\bullet OH + MB \rightarrow \text{Degradation products} \quad (7)$$

$$O_2 + MB \rightarrow \text{Degradation products} \quad (8)$$

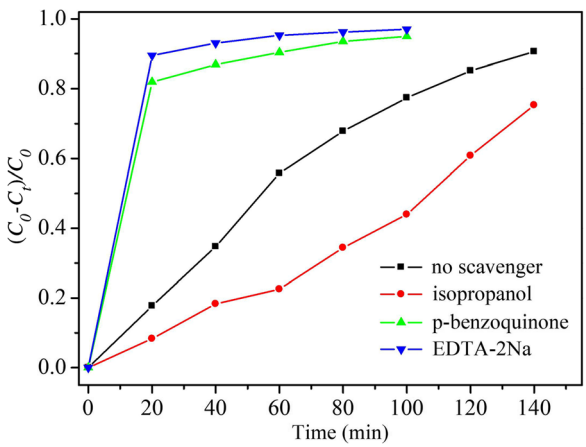

Fig. 10 Effect of various scavengers on degradation of MB

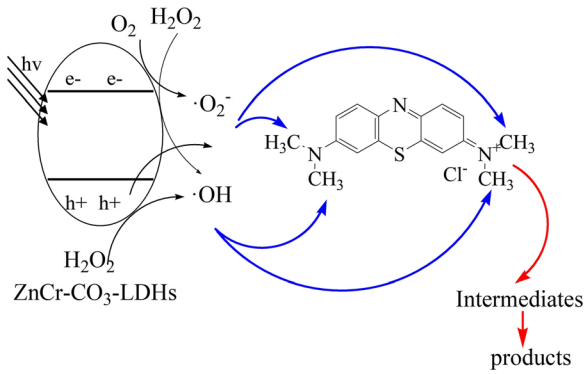

Fig. 11 Possible mechanism of photocatalytic degradation of MB using ZnCr-CO_3-LDHs

When the EDTA-2Na was added to the reaction system, the h^+ was captured, which caused Eq. 1 to move to the right, so that a large amount of photoinduced e^- formed on the catalyst surface and inside. Photoinduced e^- deoxidizes H_2O_2 and O_2 molecules to produce •OH and $\bullet O_2^-$ species on the photocatalyst surface according to Eq. 3 and Eq. 4. The •OH could oxidize MB effectively, while $\bullet O_2^-$ and H_2O_2 generated •OH and O_2 according to Eq. 6. Therefore, in the process of photocatalysis of MB, a large number of bubbles were produced in the solution, and the MB was degraded rapidly. When p-benzoquinon was added, $\bullet O_2^-$ in the solution was trapped, which caused Eq. 4 to move to the right. Subsequently, Eq. 1 and Eq. 2 were accelerated, speeding up the generation of •OH and accelerating the degradation of MB. However, one could speculate that the addition of p-benzoquinon did not capture $\bullet O_2^-$ rapidly, so that part of $\bullet O_2^-$ could react with H_2O_2 (Eq. 6). This concept is consistent with the fact that a large number of bubbles was produced in the solution during the experiment.

Based on the above discussion, combined with the analysis of UV-Vis absorption spectra, the possible mechanism of ZnCr-CO_3-LDHs photocatalytic degradation of MB was considered (Fig. 11). Under visible light irradiation, ZnCr-CO_3-LDH was excited, and its valence band electrons were transferred to the conduction band to produce photogenerated electrons (e^-) and holes (h^+). These e^- and h^+ could move freely in the catalyst. When they moved to the catalyst surface, e^- reacted with O_2 and H_2O_2 in the solution to produce $\bullet O_2^-$ and •OH, and h^+ in the valence band reacted with H_2O_2 to generate •OH. These active species then reacted with MB, causing MB to undergo demethylation, and also oxidized MB to small molecules, thus achieving the purpose of decolorization and degradation.

CONCLUSIONS

In the present study, *M*/Cr hydrotalcites (M_3Cr-CO_3-LDHs) (in which *M* = Mg, Co, Ni, Cu, or Zn), where the *M*/Cr molar ratio was 3, were prepared by the co-precipitation method. XRD and FTIR tests showed that five kinds of M_3Cr-CO_3-

https://doi.org/10.1007/s42860-019-00031-2 Published online by Cambridge University Press

LDHs were synthesized successfully, the samples obtained had regular layered structures and were single crystal phases. FTIR and TG-DTA analysis showed the M_3Cr-CO_3-LDHs to have thermal stability characteristics typical of carbonate hydrotalcites. In addition, the thermal stability was in the order: Cu_3Cr-CO_3-LDHs > Mg_3Cr-CO_3-LDHs > Ni_3Cr-CO_3-LDHs > Zn_3Cr-CO_3-LDHs ≈ Co_3Cr-CO_3-LDHs. When MB solution was exposed to ZnCr-CO_3-LDH, H_2O_2, and visible light irradiation together, more than 90.67% of the MB was removed after 140 min. Photocatalytic activity of the samples was in the order: Co_3Cr-CO_3-LDHs > Mg_3Cr-CO_3-LDHs > Cu_3Cr-CO_3-LDHs> Zn_3Cr-CO_3-LDHs >Ni_3Cr-CO_3-LDHs. The results of a reaction mechanisms study showed photocatalytic degradation of MB involved demethylation, and the reactive species contained $•O_2^-$, •OH, and h^+.

ACKNOWLEDGEMENTS

This Project is supported by Zhejiang Provincial Natural Science Foundation of China (No. LY17E040001; No. LQ19E040001).

REFERENCES

Adeleke, J. T., Theivasanthi, T., Thiruppathi, M., Swaminathan, M., Akomolafe, T., & Alabi, A. B. (2018). Photocatalytic degradation of methylene blue by ZnO/$NiFe_2O_4$ nanoparticles. *Applied Surface Science, 455*, 195–200. https://doi.org/10.1016/j.apsusc.2018.05.184.

Alijani, M., Kaleji, B. K., & Rezaee, S. (2017). Highly visible-light active with Co/Sn co-doping of TiO_2 nanoparticles for degradation of methylene blue. *Journal of Materials Science Materials in Electronics, 28*, 15345–15353. https://doi.org/10.1007/s10854-017-7420-6.

Bohac, P., & Bujdak, J. (2018). Prepublication: tuning the photophysical properties of cyanine dyes with clay minerals. *Clays and Clay Minerals, 66*, 127–137. https://doi.org/10.1346/CCMN.2018.064090.

Chen, Q., He, Q. Q., Lv, M. M., Liu, X. T., Wang, J., & Lv, J. P. (2014). The vital role of PANI for the enhanced photocatalytic activity of magnetically recyclable N–$K_2Ti_4O_9$/$MnFe_2O_4$/PANI composites. *Applied Surface Science, 311*, 230–238. https://doi.org/10.1016/j.apsusc.2014.05.046.

Chen, Y. F., Bao, Y., & Wang, X. Q. (2016). Green emission of Tb-doped Mg-Al layered double hydroxide response to L-lysine. *Journal of Fluorescence, 26*, 813–820. https://doi.org/10.1007/s10895-016-1769-4.

Comelli, N. A., Ruiz, M. L., Aparicio, M. S. L., Merino, N. A., & Ponzi, M. I. (2018). Influence of the synthetic conditions on the composition, morphology of cumgal hydrotalcites and their use as catalytic precursor in diesel soot combustion reactions. *Applied Clay Science, 157*, 148–157. https://doi.org/10.1016/j.clay.2018.02.039.

Crossland, E. J. W., Noel, N., Sivaram, V., Leijtens, T., Alexander-Webber, J. A., & Snaith, H. J. (2013). Mesoporous TiO_2 single crystals delivering enhanced mobility and optoelectronic device performance. *Nature, 495*, 215–219. https://doi.org/10.1038/nature11936.

Da, S. E., Prevot, V., Forano, C., Wong-Wah-Chung, P., Burrows, H. D., & Sarakha, M. (2014). Heterogeneous photocatalytic degradation of pesticides using decatungstate intercalated macroporous layered double hydroxides. *Environmental Science & Pollution Research International, 21*, 11218–11227. https://doi.org/10.1007/s11356-014-2971-z.

Fu, S., Zheng, Y., Zhou, X., Ni, Z., & Xia, S. (2019). Visible light promoted degradation of gaseous volatile organic compounds catalyzed by au supported layered double hydroxides: influencing factors, kinetics and mechanism. *Journal of Hazardous Materials, 363*, 41–54. https://doi.org/10.1016/j.jhazmat.2018.10.009.

Gao, Z., Sasaki, K., & Qiu, X. (2018). Structural memory effect of Mg-Al and Zn-Al layered double hydroxides in the presence of different natural humic acids: process and mechanism. *Langmuir, 34*, 5386–5395. https://doi.org/10.1021/acs.langmuir.8b00059.

Hibino, T., Yamashita, Y., Kosuge, K., & Tsunashima, A. (1995). Decarbonation behavior of Mg-Al-CO_3 hydrotalcite-like compounds during heat treatment. *Clays and Clay Minerals, 43*, 427–432. https://doi.org/10.1346/CCMN.1995.0430405.

Ishibashi, K., Fujishima, A., Watanabe, T., & Hashimoto, K. (2000). Quantum yields of active oxidative species formed on TiO_2, photocatalyst. *Journal of Photochemistry & Photobiology A Chemistry, 134*, 139–142. https://doi.org/10.1016/S1010-6030(00)00264-1.

Karataş, D.˙z., Senol-Arslan, D., & Ozdemir, O. (2018). Experimental and atomic modeling of the adsorption of acid azo dye 57 to sepiolite. *Clays and Clay Minerals, 66*, 426–437. https://doi.org/10.1346/CCMN.2018.064109.

Kuzyaka, D., Galioglu, S., Altın, İ., Sökmen, M., & Akata, B. (2018). The effect of microporous vanadosilicate Am-6 thin films as photocatalysts for the degradation of methylene blue. *Journal of Photochemistry & Photobiology A Chemistry, 366*, 127–135. https://doi.org/10.1016/j.jphotochem.2018.03.041.

Li, P., Yu, F., Altaf, N., Zhu, M., Li, J., Dai, B., & Wang, Q. (2018). Two-dimensional layered double hydroxides for reactions of methanation and methane reforming in C1 Chemistry. *Materials, **11***, 221–246. https://doi.org/10.1016/j.electacta.2017.12.139.

Mao, N., Zhou, C. H., Tong, D. S., Yu, W. H., & Cynthia Lin, C. X. (2017). Exfoliation of layered double hydroxide solids into functional nanosheets. *Applied Clay Science, 144*, 60–78. https://doi.org/10.1016/j.clay.2017.04.021.

Pan, G. X., Cao, F., Ni, Z. M., Li, X. N., Chen, H. F., Tang, P. S., & Xu, M. H. (2011). Preparation of NiMgAl layered double hydroxides and hydrogen production from aqueous-phase reforming of ethylene glycol. *Journal of the Chinese Ceramic Society, 39*, 585–589. https://doi.org/10.5535/arm.2011.35.3.427.

Pan, G. X., Ni, Z. M., Cao, F., & Li, X. N. (2012). Hydrogen production from aqueous-phase reforming of ethylene glycol over Ni/Sn/Al hydrotalcite derived catalysts. *Applied Clay Science, 58*, 108–113. https://doi.org/10.1016/j.clay.2012.01.023.

Pan, X., Wang, L. J., Sun, X. Q., Xu, B. H., & Wang, X. (2013). Ternary Titania–Cobalt Ferrite–polyaniline nanocomposite: a magnetically recyclable hybrid for adsorption and photodegradation of dyes under visible light. *Industrial & Engineering Chemistry Research, 52*, 10105–10113. https://doi.org/10.1021/ie400739e.

Prevot, V., Forano, A., & Besse, J. P. (2005). Hydrolysis in polyol: new route for hybrid-layered double hydroxides preparation. *Chemistry of Materials, 17*, 6695–6701. https://doi.org/10.1021/cm050581x.

Ray, S. K., Dhakal, D., Kshetri, Y. K., & Lee, S. W. (2017). Cu-α-$NiMoO_4$ photocatalyst for degradation of Methylene blue with pathways and antibacterial performance. *Journal of Photochemistry & Photobiology A Chemistry, 348*, 18–32. https://doi.org/10.1016/j.jphotochem.2017.08.004.

Rives, V., Prieto, O., Dubey, A., & Kannan, S. (2003). Synergistic effect in the hydroxylation of phenol over CoNiAl ternary hydrotalcites. *Journal of Catalysis, 220*, 161–171. https://doi.org/10.1016/S0021-9517(03)00245-8.

Sels, B. F., De Vos, D. E., & Jacobs, P. A. (2001). Hydrotalcite-like anionic clays in catalytic organic reactions. *Catalysis Reviews, 43*, 443–488. https://doi.org/10.1081/CR-120001809.

Shang, Y., Xi, C., Liu, W., Tan, P., Chen, H., Wu, L., & Pan, J. (2017). Photocorrosion inhibition and high-efficiency photoactivity of porous g-C_3N_4/Ag_2CrO4 composites by simple microemulsion-assisted co-precipitation method. *Applied Catalysis B Environmental, 204*, 78–88. https://doi.org/10.1016/j.apcatb.2016.11.025.

Tichit, D., Gerardin, C., Durand, R., & Coq, B. (2006). Layered double hydroxides: precursors for multifunctional catalysts. *Topics in Catalysis, 39*, 89–96. https://doi.org/10.1007/s11244-006-0041-6.

Vialat, P., Leroux, F., Taviot-Gueho, C., Villemure, G., & Mousty, C. (2013). Insights into the electrochemistry of $(Co_xNi_{(1-x)})_2Al–NO_3$ layered double hydroxides. *Electrochimica Acta, 107*, 599–610. https://doi.org/10.1016/j.electacta.2013.06.033.

Wang, L., Wang, D., Dong, X. Y., Zhang, Z. J., Pei, X. F., Chen, X. J., & Jin, J. A. (2011). Layered assembly of graphene oxide and Co-Al layered double hydroxide nanosheets as electrode materials for supercapacitors. *Chemical Communications, 47*, 3556–3668. https://doi.org/10.1039/c0cc05420h.

Xia, S. J., Liu, F. X., Ni, Z. M., Shi, W., Xue, J. L., & Qian, P. P. (2014). Ti-based layered double hydroxides: efficient photocatalysts for azo dyes degradation under visible light. *Applied Catalysis B: Environmental, 144*, 570–579. https://doi.org/10.1016/j.apcatb.2013.07.060.

Xiang, Q., Yu, J., & Wong, P. K. (2011). Quantitative characterization of hydroxyl radicals produced by various photocatalysts. *Journal of Colloid & Interface Science, 357*, 163–167. https://doi.org/10.1016/j.jcis.2011.01.093.

Xiong, P., Chen, Q., He, M. Y., Sun, X. Q., & Wang, X. (2012). Cobalt ferrite–polyaniline heteroarchitecture: a magnetically recyclable photocatalyst with highly enhanced performances. *Journal of Materials Chemistry, 22*, 17485–17493. https://doi.org/10.1039/C2JM31522J.

Xu, M., Pan, G., Meng, Y., Guo, Y., Wu, T., & Chen, H. (2019). Effect of Ce3+ on the photocatalytic activity of MAlCe ternary hydrotalcites-like compounds in methylene blue photodegradation. *Applied Clay Science, 170*, 46–56. https://doi.org/10.1016/j.clay.2019.01.011.

Yang, Z. H., Qian, W. M., Chu, Y. M., & Zhang, W. (2018). On approximating the arithmetic-geometric mean and complete elliptic integral of the first kind. *Journal of Mathematical Analysis and Applications, 462*, 1714–1726. https://doi.org/10.1016/j.jmaa.2018.03.005.

Yang, Z. H., Chu, Y. M., & Zhang, W. (2019). High accuracy asymptotic bounds for the complete elliptic integral of the second kind. *Applied Mathematics and Computation, 348*, 552–564. https://doi.org/10.1016/j.amc.2018.12.025.

Yuan, B., Wei, J., Hu, T., Yao, H. B., Jiang, Z. H., Fang, Z. W., & Chu, Z. Y. (2015). Simple synthesis of g-C_3N_4/rGO hybrid catalyst for the photocatalytic degradation of rhodamine B. *Chinese Journal of Catalysis, 36*, 1009–1016. https://doi.org/10.1016/S1872-2067(15)60844-0.

Zhang, T. Y., Oyama, T., Aoshima, A., Hidaka, H., Zhao, J. C., & Serpone, N. (2001). Photooxidative n-demethylation of methylene blue in aqueous TiO_2 dispersions under UV irradiation. *Journal of Photochemistry & Photobiology A Chemistry, 140*, 163–172. https://doi.org/10.1016/S1010-6030(01)00398-7.

Zhang, X., Wang, L., Zhou, X., Ni, Z., & Xia, S. (2018). Investigation into the enhancement of property and the difference of mechanism onto visible light degradation of gaseous toluene catalyzed by ZnAl layered double hydroxides before and after Au supporting. *ACS Sustainable Chemistry & Engineering, 6*, 13395–13407. https://doi.org/10.1021/acssuschemeng.8b03186.

Zhao, Y. F., Zhang, S., Li, B., Yan, H., He, S., Tian, L., & Duan, X. (2011). A Family of Visible-Light Responsive Photocatalysts Obtained by Dispersing CrO_6 Octahedra into a Hydrotalcite Matrix. *Chemistry -A European Journal, 17*, 13175–13181. https://doi.org/10.1002/chem.201101874.

Zhou, C. H. (2010). Emerging trends and challenges in synthetic clay-based materials and layered double hydroxides. *Applied Clay Science, 48*, 1–4. https://doi.org/10.1016/j.clay.2009.12.018.

Zhou, C. H. & Keeling, J. (2013). Fundamental and applied research on clay minerals: from climate and environment to nanotechnology. Applied Clay Science, 74, 3–9. .https://doi.org/10.1016/j.clay.2013.02.013

Zhou, C. H., Li, Z. Z., Ai, Q. W., Tian, H. C., & Hong, P. H. (2016). Current fundamental and applied research into clay minerals in china. *Applied Clay Science, 119*, 3–7. https://doi.org/10.1016/j.clay.2015.07.043.

(Received 31 January 2019; revised 27 July 2019; AE: Chun-Hui Zhou)